Electrochemical Performance of Metal-Free Carbon-Based Catalysts from Different Hydrothermal Carbonization Treatments for Oxygen Reduction Reaction

Claudio Fontanesi *, Andrea Marchetti, Massimo Innocenti, Roberto Giovanardi, Aldo Girimonte, Andrea Stefani, Clara Mucci

Posted Date: 13 December 2023

doi: 10.20944/preprints202312.0971.v1

Keywords: ORR catalysts; hydrothermal treatment; glucose; nanostructures

Article

Electrochemical Performance of Metal-Free Carbon-Based Catalysts from Different Hydrothermal Carbonization Treatments for Oxygen Reduction Reaction

Aldo Girimonte [1], Andrea Stefani [2], Clara Mucci [1], Roberto Giovanardi [1], Andrea Marchetti [3], Massimo Innocenti [4,5] and Claudio Fontanesi [1,5,*]

[1] University of Modena and Reggio Emilia, Department of Engineering, DIEF, via vivarelli 10, 41125 Modena, ITALY;
[2] University of Modena and Reggio Emilia, Department of Physics, FIM, via Campi 213, 41125 Modena, ITALY
[3] University of Modena and Reggio Emilia, Department of Chemical and Geological Science, DSCG, via Campi 103, 41125 Modena, ITALY
[4] University of Firenze, Department of Chemistry, "Ugo Schiff", via della Lastruccia 3, 50019 Sesto Fiorentino, ITALY
[5] National Interuniversity Consortium of Materials Science and Technology (INSTM), Via G. Giusti 9, 50121 Firenze, ITALY
* Correspondence: claudio.fontanesi@unimore.it

Abstract: This research investigates the difference on the products obtained through two hydrothermal carbonization treatments. Our aim is to synthesize metal-free, carbon-based catalysts for the Oxygen Reduction Reaction (ORR) to serve as efficient and cost-effective alternatives to platinum-based catalysts. Catalysts synthesized using the traditional hydrothermal approach exhibit a higher electrocatalytic activity for ORR in alkaline media, despite a more energy-intensive production process. The superior performance is attributed to differences in particle morphology and to the chemical composition of the particle surfaces. The presence of functional groups on the surfaces of catalysts obtained via traditional approach significantly enhances ORR activity by facilitating deprotonation reactions in an alkaline environment. Our research aims to be a reference for future investigations, shifting the focus to the fine-tuning of surface chemical compositions and morphologies of metal-free catalysts to enhance ORR activity.

Keywords: ORR catalysts; hydrothermal treatment; glucose; nanostructures

1. Introduction

The Oxygen Reduction Reaction (ORR) has gained significant attention in recent years. ORR is the electrochemical process where molecular oxygen is reduced, typically forming water in acidic environment or hydroxide ions in alkaline environments. This reaction assume a significant role for energy conversion devices, including fuel cells, metal-air batteries and electrolyzers [1] [2]. As the global push for sustainable and renewable energy solutions increase, the efficient and cost-effective conversion and storage of energy have become fundamental topics for scientific researches.

The ORR is a sluggish reaction and has been often catalyzed by precious metals, with platinum (Pt) being the most effective [3] [4]. However, the prohibitive cost, scarcity, and sustainability associated with Pt and other noble metals drag the research for alternatives. Among all, carbon-based metal-free catalysts has shown promising properties in alkaline environment [5] [6] [7] especially if focusing on the prospect of high performance at a fraction of the cost and with wide availability of resources. These materials also show some obstacle in the path of commercial utilization, with issues related mainly to their long-term stability, selectivity, and kinetics often in contrast to their noble

 doi:10.20944/preprints202312.0971.v1

metal counterparts [8]. Furthermore, the wide variety of carbon materials, from graphene to carbon nanotubes to amorphous carbons, means that a one-size-fits-all approach is usually not possible [9] [10] [11].

A particularly promising strategy to obtain catalysts with high carbon content and controllable nanostructures is the Hydrothermal Carbonization Technique (HTC). HTC is based on the treatment of aqueous solutions of both organic and inorganic precursors at elevated temperatures and pressures and allows for the fabrication of carbon materials with higly tunable properties by adjusting parameters like temperature, time, and precursor composition. Several works have highlighted the efficacy of HTC-derived carbon materials [12] [13].

Traditional HTC (T-HTC), conducted using standard ovens as energy source, while effective, is often energy-intensive, but an alternative path can be identified in MicroWave-ssisted HTC (MW-HTC), promising a significant reductions in energy consumption and process time [14]. A comprehensive comparison of these synthesis methods, with an evaluation from the energy efficiency of the production process to catalyst performance, has been missing in recent studies. Therefore, in our research we addressed this gap, aiming to underline both the advantages and drawbacks of products obtained through Traditional and MicroWave-assisted HTCs.

2. Materials and Methods

2.1. Reagents

The initial solutions are prepared using D-(+)-Glucose (≥99.5%, Sigma-Aldrich) as the solute and millipore distilled water as the solvent. Potassium hydroxyde KOH white pellets (≥85%, white pellets, Sigma-Aldrich), Poly(vinylidene fluoride) PVDF (average Mw ~534,000 by GPC, powder, Sigma-Aldrich), 1-Methyl-2-pyrrolidone NMP (99%, Sigma-Aldrich) were used in the characterization stages.

2.2. Experimental

2.2.1. T-HTC

In the conventional hydrothermal method (T-HTC), the synthesis start with the preparation of a 1M D-(+)-glucose aqueous solution, which is poured in a stainless steel autoclave which is internally equipped with a Teflon liner filling up to 60% of the total volume. The autoclave is then sealed and positioned within a controlled oven and using convection heating. The synthesis is carried out with a set temperature of 190°C with a isothermal of 15 hours. Upon conclusion of the reaction, a filtration procedure is used to separate the dark precipitate. After this step, the solid precipitate is dried at temperature of 70°C for a minimum duration of 24 hours.

2.2.2. MW-HTC

For this synthesis, aqueous solutions of D-(+)-glucose were formulated with varying molar concentrations: 0.1 M, 0.3 M, 0.5 M and 1 M. Utilizing the capabilities of the machine (model "Milestone ultraWAVE"), which can allow simultaneous hydrothermal treatments, 20 ml of each prepared solution was poured into individual quartz containers, and each container was then positioned within a vessel containing 120 ml of tap water. All solution were inserted into the machine's housing and hermetically sealed. The machine is connected to nitrogen gas (N_2) and pressurized to 31.5 bar. The machine's operational protocol involves achieving a target temperature within a 15 minute cycle, followed by the synthesis phase where it sustains an internal temperature of 190°C and pressure of 120 bar for a duration of 30 minutes [14] [15] [16]. After complete system cooldown, the resultant solutions are extracted.

The phase separation in this method has demonstrated more challenges than in the conventional HTC synthesis, as filtration was ineffective due to the apparent small size of the precipitate that remains inseparable with very low amount of residues. To address this, the samples undergo a centrifugation at 4500 rpm for 20 minutes that facilitate the segregation of synthesized particles.

 doi:10.20944/preprints202312.0971.v1

Nonetheless, this separation technique was effective only for concentrations exceeding 0.5 M, while concentrations below this threshold yield minimal material residues that cannot be used for electrochemical or physical characterization. Subsequently the obtained particles undergo a drying process at 70°C for 24 hours.

2.2.3. Characterization

An initial physical characterization of the separated particles was conducted using SEM microscopy. The 1M concentration samples were examined focusing on particles derived from MW-HTC in comparison to those from T-HTC. The 1M concentration was selected because these samples were the only ones effectively separated in usable amounts and also had a precursor solution concentration that was comparable.

To evaluate the ORR-catalytic capabilities of particles derived from diverse glucose syntheses, we conducted electrochemical tests using a Rotating Disk Electrode (RDE) connected to an electrochemical cell via a potentiostat. The electrode construction is based on Au substrate and prior to drop-casting each substrate is cleaned, starting from a polishing step using a porous disk saturated with a fine Al_2O_3 ceramic oxide suspension, then followed by a gentle flame annealing process with ethanol flame. Solutions containing the synthesized particles were prepared and subsequently drop casted on the Au electrode's surface using a controlled volume micropipette for mass loading control. The drop casting solution comprised glucose nanospheres suspended in 5% PVDF solution in NMP, and the obtained wet electrode was treated through a vacuum drying process at 120°C to eliminate solvent traces, achieving a final mass loading of 5 mg/cm2.

The dried electrode was used to build the electrochemical cell, serving as the working electrode (WE) connected to the RDE, which determines its rotational velocity. The setup also incorporated an Ag/AgCl wire as the reference electrode (RE) and a Pt wire as the counter electrode (CE). Experiments were executed by submerging the WE in a 0.1 M KOH solution and rotating it at various engine speeds (500, 1000, 1500, 2000, 2500, and 3000 rpm). Simultaneously, either O_2 or Ar was fluxed into the solution to achieve oxygen-saturated or oxygen-depleted conditions, respectively. Several Linear Sweep Voltammetry (LSV) tests were conducted on the samples, with each test incrementally elevating the RDE's rotational speed. Comparative analysis of the LSV curves derived from 1M D-(+)-glucose precursor was performed to highlight the impact of a polycondensation process via traditional hydrothermal treatment versus microwave-assisted approaches.

To further characterize the products synthesized via conventional and microwave-assisted hydrothermal carbonization methods, Fourier Transform Infrared Spectroscopy (FTIR) analysis was conducted. For this purpose a Vertex 70 FTIR spectrophotometer was used, with a detector kept under control by a liquid nitrogen cooling system, working in Attenuated Total Reflection (ATR) mode with air flow inside the system.

This technique allows to analyze solid samples by applying a relatively simple preparation, placing them directly in contact with a component with a high refractive index. The light beam generated by the source is passed through the sample and the optical element, with a series of reflections that allow the instrument to develop an IR spectrum of the sample. By exploiting the characteristics of the evanescent wave the detector is able to generate curves as a functions of wavelength and transmittance; they are subsequently expressed in the final graph with respect to absorbance to facilitate the graph reading.

The experiment was conducted by first creating a "blank" IR spectrum of the ATR system, in order to obtain an appropriate baseline. Subsequently, the IR spectrum of three different solid samples were obtained:

1. Pure Glucose (D-(+)-glucose)
2. Carbonaceous nanostructures obtained from 1M glucose solution using hydrothermal carbonization (T-HTC)
3. Carbon nanospheres acquired from 1M glucose solution by microwave-assisted hydrothermal carbonization (MW-HTC)

 doi:10.20944/preprints202312.0971.v1

3. Results and discussion

3.1. Synthesis processes

Following the conclusion of the synthesis, our initial step was a visual qualitative inspection of the products obtained. The wet product suspension resulting from the T-HTC exhibited a gelatinous consistency, resembling caramel in terms of dark color. This property can be attributed to the emergence of insoluble particles obtained from glucose polycondensation. These products of synthesis, subjected to filtration and subsequent drying, transformed into dark powders which was then used for further characterization. Upon visual examination of the MW-HTC process results, it was observed that the clear solutions evolved into dark-brown suspensions, with darker colors proportional to the precursor concentration. Centrifugation yielded a wet precipitate with a gel-like consistency, with lots of difficulties in separating and washing particles from suspension with precursor that was under 0.5 M. We further observed that despite a drying period exceeding 24 hours, the particle obtained from centrifugation of MW-HTC retained a caramel-like consistency. This contrasted with the products obtained via the T-HTC, which were easily manipulated and transformed into dry powders for subsequent experimental procedures.

Our hypothesis attributes these behaviors of the synthesis products to the growth phase at which particles are extracted during polycondensation, which in turn influences their morphology and surface chemistry. Various mechanisms have been postulated in several articles [15] [13] [17] for the polycondensation of carbohydrates, and the possible critical phases for D-(+)-glucose can be outlined as the following:

1. **Initiation**: D-(+)-glucose undergoes hydrolysis in hydrothermal conditions (elevated solvent temperatures at the vessel's high pressures), driven by hydronium ions from the autoionization of water.
2. **Production of Soluble Derivatives**: The advancing hydrolysis yields different soluble derivatives and various acids. Among these products there are fructose, furfurals (such as 5-hydroxymethylfurfural, 5 HMF), carboxylic acids (formic, acetic, levulinic, etc.), aldehydes (formic, acetic, etc.), while H_2, CO_2, CO and various light hydrocarbons (methane, ethane, propane, etc) can be distinguished in the gaseous phase. The resulting acids, especially those deriving from monosaccharide degradation, serve dual purposes as they catalyze further reactions and become foundational elements during latter microstructures growth.
3. **Polymerization**: The soluble derivatives enter reactions of polymerization through mechanisms like intermolecular dehydration and aldol condensation. Concurrently, there's a potential for these polymers to undergo aromatization, resulting in aromatic clusters. When these clusters attain a saturation threshold, they trigger a nucleation event.
4. **Progressive Growth and Settling**: Originating nuclei undergo growth driven by the dehydration of aromatic products. As they grow their solubility diminishes, making them increasingly hydrophobic leading them to precipitate.
5. **Particle Clustering**: These hydrophobic particles tend to cluster together, pushing to minimize surface energy. During this phase, carbon-rich spheres separate from the hydrothermal water. The latter development is accentuated by high temperature processes and alkaline catalysts, while being inhibited by a high concentration of glucose. Once their growth reaches a plateau, the outer surfaces of these microstructures exhibit reactive functional groups, while the inner core is composed by more stable carbon-rich groups.

Variables such as the precursor solution concentration, the reaction temperature and the duration have demonstrated a pronounced effect on the product [5] [14] [6]. Elevated reactant concentrations amplify the polymerization process, yielding uniformly shaped microspheres while higher temperatures and longer durations lean towards higher carbonization degrees, resulting in nanospheres of irregular geometries and a reduced presence of surface oxygen-rich functional groups [18].

Preprints (www.preprints.org) | NOT PEER-REVIEWED | Posted: 13 December 2023 doi:10.20944/preprints202312.0971.v1

We hypothesize that the difference in tackiness exhibited by the samples from the two methods can be traced back to variations in surface chemistry, particle size, hydrophobicity and related hygroscopicity.

In fact, the hygroscopic nature of particles can be linked to their size and hydrophobic characteristics. Smaller particles, with their larger surface-to-volume ratios, offer more active sites for moisture adsorption, rendering them inherently more hygroscopic than their larger counterparts. This heightened hygroscopicity is further influenced by the density of functional groups present on the particle's surface. The more surface area available, the higher the specific density of hydrophilic functional groups, which can attract and retain water molecules. This difference might be amplified by the potential synergistic effects of the microwaves on the HTC process, which could result in a lesser degree of carbonization. The microwave-assisted method is renowned for its rapid and uniform energy distribution to reactants, achieved through induction of the oscillation of polar groups like hydroxyl and carbonyl, resulting in heat generation. The possibility that certain surface groups formed during glucose polycondensation act as focal points for this energy transfer could lead to localized changes in reaction kinetics and surface affinities of the products. To understand the product properties and their relationship with morphological characteristics, comprehensive characterizations, including SEM imaging and FTIR analysis, have been performed.

3.2. Physical characterization

We turned to SEM microscopy to visually assess the morphology of the synthesized particles. The SEM images, presented in Figure 1, sustain our observations regarding the differences in particle sizes resulting from the two synthesis methods. In Figure 1.a, particles synthesized via T-HTC are shown. Upon first examination, a marked lack of uniformity in particle size was evident in the samples produced by T-HTC. Additionally, several particles are seen in the process of neck formation, an indication of agglomeration during growth leading to larger particle sizes. In contrast, Figure 1.b show particles synthesized via MW-HTC. Here, the size distribution is uniform across the sample, with no significant neck formation.

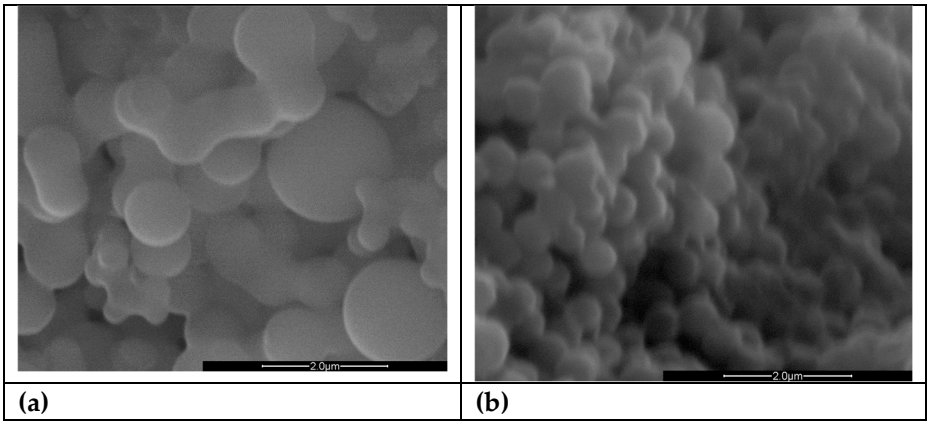

Figure 1. SEM images of carbon nanosphere derived from HTC treatment of D-(+)-glucose (1 M) obtained by (**a**) T-HTC and (**b**) MW-HTC.

Image analysis was employed to define the particle size distribution, and the results have been reported in Table 1. The particles derived from MW-HTC exhibit a narrow size distribution, while those synthesized by traditional methods display a broader range of sizes. These findings support our hypothesis that MW-HTC leads to a more controlled and uniform particle growth, which in turn defines the surface properties.

Preprints (www.preprints.org) | NOT PEER-REVIEWED | Posted: 13 December 2023 doi:10.20944/preprints202312.0971.v1

Table 1. Results obtained from SEM image analysis for particle surface and form factor measurement.

	Traditional HTC	MW-HTC
Surface average (µm²)	4.46	1.57
Sigma surface (µm²)	3.70	0.40
Form factor average	1.05	1.06
Sigma Form factor	0.09	0.05

3.3. Electrochemical characterization

Electrochemical characterization of the synthesized products was carried out initially preparing and testing our experimental setup under two distinct conditions to establish a baseline for comparison. The initial trials were conducted with a gold (Au) bare electrode immersed in a 0.1M KOH solution. This system was purged with argon for a minimum of one hour to ensure low oxygen content. Subsequently, we replicated the experimental setup but altered the environment by saturating the electrolyte with air, thereby introducing a substantial oxygen presence. The outcomes of these experiments are illustrated in Figure 2.

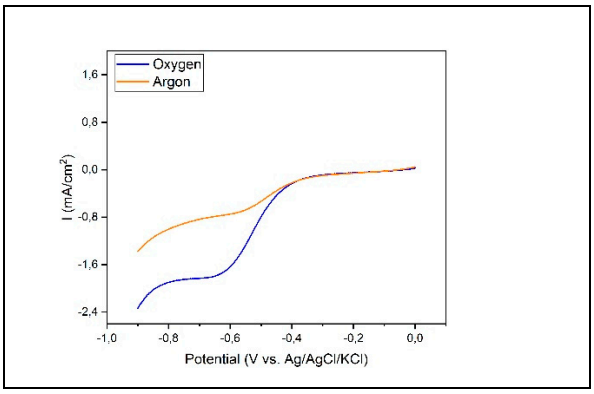

Figure 2. LSV of bare Au electrode as blank test in de-oxygenated and oxygen saturated in 0.1M KOH.

It is evident that no significant reduction current manifests until reaching a potential onset near -0.3 V for both scenarios. At this potential we observe a reduction peak which is attributed to the Oxygen Reduction Reaction (ORR). Despite the argon purge, a residual amount of oxygen remains in the deaerated solution, although less than in the air-saturated one. Further exploration into the voltage window reveals an additional onset of reduction beginning at approximately -0.8 V, which we ascribe to the evolution of hydrogen gas (HER), in aligment with the thermodynamic potentials associated with this reaction in alkaline environment. These observations enabled us to establish potential window for the investigation of ORR in our system from -0.1 to -0.7 V when applying the catalyst as WE.

In Figure 3.a, the catalysts derived from T-HTC displayed the expected behavior for ORR. The onset potential for ORR increased if compared to the blank test, affirming the catalytic advantage of the catalysts over simple gold substrates. Moreover, as the RDE's rotation speed was increased, a corresponding rise in limiting current was observed, suggesting enhanced mass transport of oxygen to the electrode surface. The particles synthesized by MW-HTC exhibited an worse response during the RDE testing, showing only a marginal enhancement of the limiting current during an increase in the rotation speed. This behavior was further analyzed, and the data extracted for half-wave potential and limiting current are presented in Levich plot in Figure 3.d, offering a visual representation of the rotation-dependent behavior. While the T-HTC particles maintain a pronounced dependency on the rotation rate with a slope of $-1.52*10^{-5}$ A $(rad/s)^{-1/2}$, indicating expected Levich behavior and good electrochemical performance through ORR, the MW-HTC particles show a flatter slope and reduced current values with only $-5.10*10^{-7}$ A $(rad/s)^{-1/2}$. A steeper Levich plot slope indicates a more efficient

Preprints (www.preprints.org) | NOT PEER-REVIEWED | Posted: 13 December 2023 doi:10.20944/preprints202312.0971.v1

process, suggesting that the oxygen molecules are being reduced at the electrode surface more readily in the T-HTC samples. T-HTC particles outperform MW-HTC in ORR efficiency, so there is a distinct electrochemical phenomenon at play that influences the reactivity and catalytic properties of the ORR on the particle surfaces.

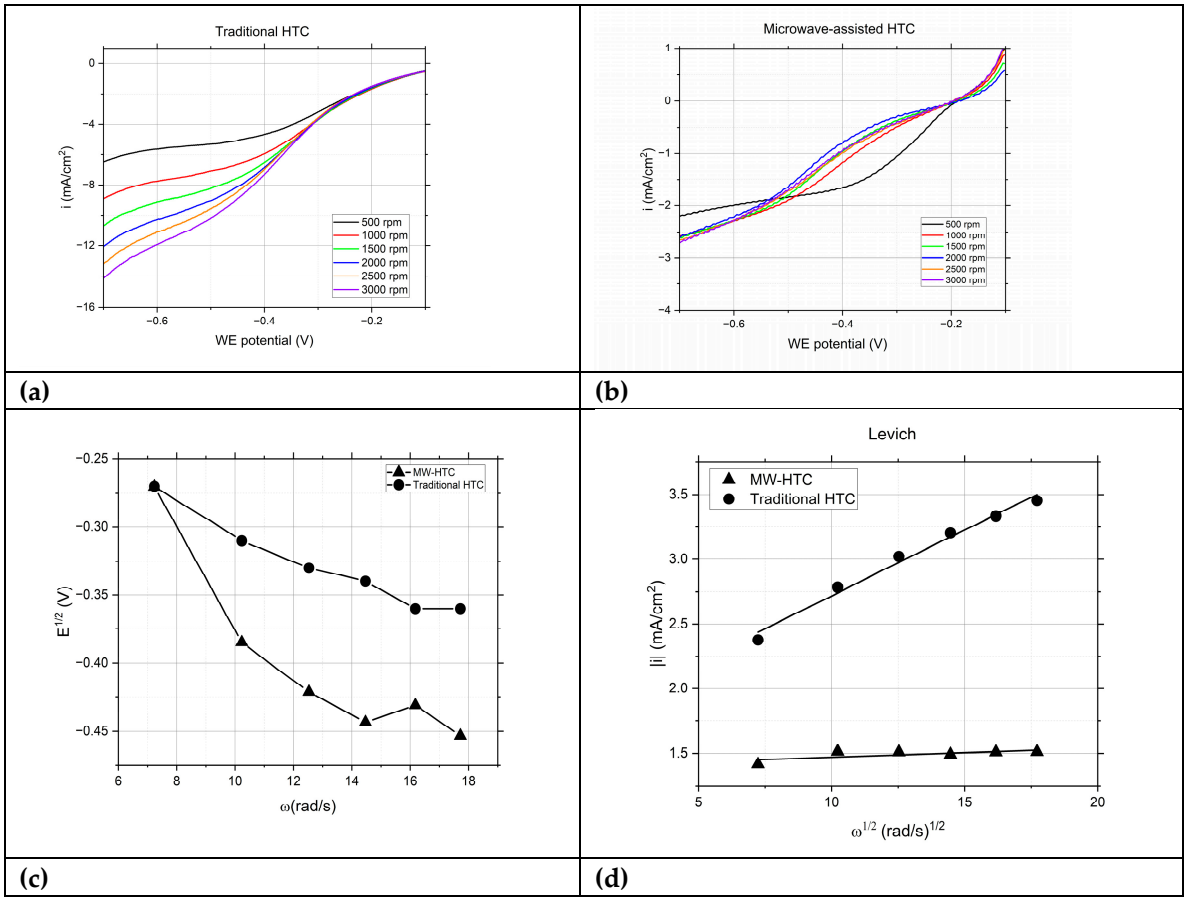

Figure 3. (**a**) LSV of T-HTC catalyst, (**b**) LSV of MW-HTC catalyst (**c**) comparison of half wave potentials (**d**) comparison of Levich plots.

To determine the effective area on the surface of the electrode where the reactions for both T-HTC and MW-HTC particles take place, Levich's equation (Eq.01) was applied from the experimental data obtained:

$$i_l = 0.62 * n * F * A * D^{2/3} * \omega^{1/2} * C_0 * \nu^{-1/6} \quad (1)$$

where the number of electrons exchanged n is equal to 1, F is Faraday's constant, A is the area of the electrode to be determined; the diffusion coefficient of Oxygen D results in aqueous solution at 25 °C equal to 0.00242 mm²/s, C0 is the concentration of Oxygen in the bulk of the solution equal to 1.22x10^{-9} mol/mm³ while the kinematic viscosity υ is equal to 0.9132 mm²/s. The calculation was carried out considering values of angular velocity of the electrode ω within a range of [500; 3000] rpm and current values relative to the potentials -0.55 V and -0.7 V, which represent the reference extremes of the potential range of interest. The determined A values are explained in Table 2:

Table 2. Variation of electrode surface as a function of rotational speed and current at potential values of -0.55V and -0.7V.

Effective Area [mm²]			
I [A] T-HTC at -0.55V	I [A] T-HTC At -0.7V	I [A] MW-HTC at -0.55V	I [A] MW-HTC at -0.7V
3.32 x10^4	4.58 x10^4	2.63 x10^2	2.54 x10^3

Preprints (www.preprints.org) | NOT PEER-REVIEWED | Posted: 13 December 2023 doi:10.20944/preprints202312.0971.v1

Our hypothesis is that the MW-HTC particles might facilitate an alternative reduction reaction concurrent with ORR, happening in the active material itself. This side reaction could be altering the active sites on the material's surface, thus limiting the expected increase in ORR current with higher rotation speeds.

To investigate these chemical differences, infrared (IR) spectroscopy analyses were conducted. By examining the IR spectra, we can identify the presence and density of various functional groups that contribute to the electrocatalytic activity, such as hydroxyl, carbonyl, and carboxylic groups.

3.4. Infrared Spectroscopic Analysis

Figure 4 displays IR spectra of the carbon-based particles synthesized both via the slow T-HTC and the more rapid MW-HTC. These are compared with the spectrum of pure D-glucose, represented by the black trace (panel a).

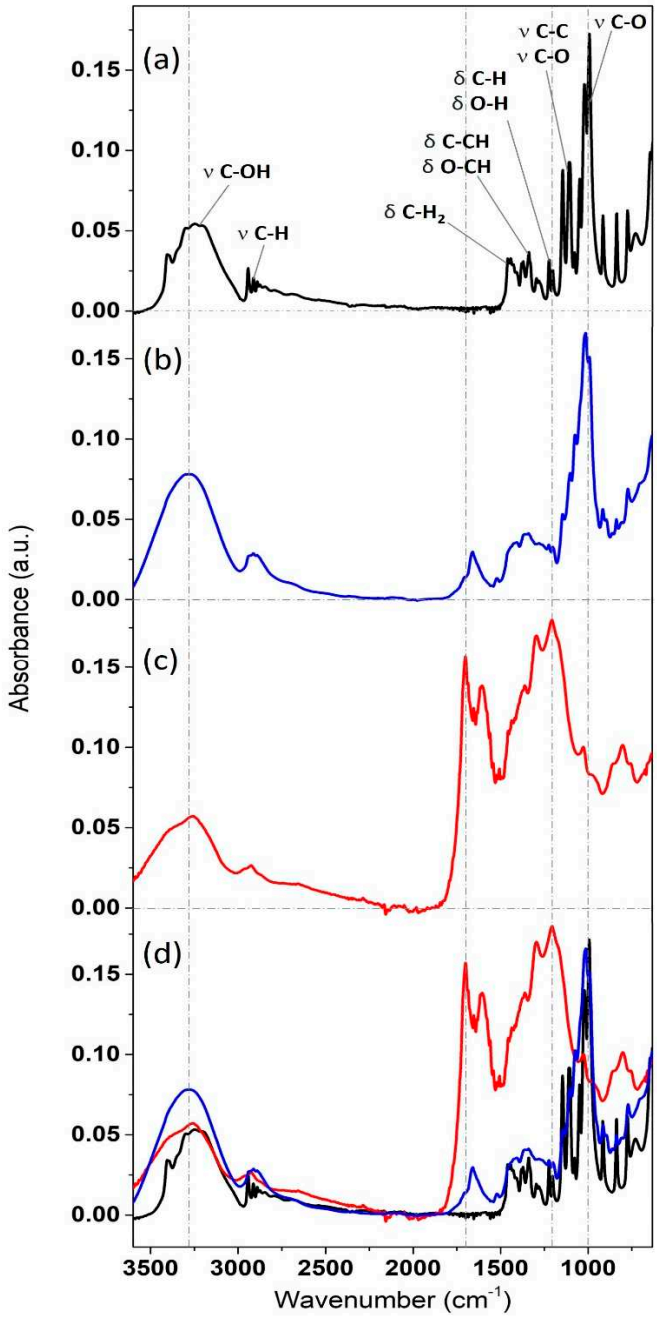

Figure 4. IR spectra of three different samples (a) D-(+)-glucose (**b**) MW-HTC (**c**) T-HTC and (**d**) overlapped.

 doi:10.20944/preprints202312.0971.v1

The IR bands of the D-(+)-glucose reagent are in perfect agreement with the scientific literature [19]. Proceeding in decreasing energy, the broad absorption peak extending from 3500 to 3000 cm^{-1} is assigned to the C-O stretching of alcohol groups [20]. The breadth of the structure is due to the presence of signals from both the four secondary alcohol groups and the primary alcohol group (linked to the methylene group). The signals at 2900 cm^{-1} are ascribed to C-H and C-H_2 stretching vibrations (the latter related to the methylene group). The bands between 1480 and 1400 cm^{-1} are associated with CH_2 and C=O bending (scissoring, δ) [21]. The region from 1380 to 1300 cm^{-1} refers to scissoring motions involving carbon, especially C-CH and O-CH. The two bands between 1230 and 1185 cm^{-1} are attributed to CH and OH bending, while subsequently, a series of high-intensity peaks can be assigned to C-O and C-C stretching vibrations. In particular, the C-O stretching vibrations up to around 1050 cm^{-1} are related to the four secondary alcohol groups, while the high-intensity peak dominating the spectrum at 1020 cm^{-1} is assigned to the C-O of the primary alcohol group [22].

In comparison to what has been presented, the spectra of the heat-treated particles are intensity-normalized to the C-H stretching band at 2900 cm^{-1}, since these bonds have only a marginal influence on the polycondensation reaction. This procedure leads to the subsequent natural coincidence in the absorption of the CH_2 band at 600 cm^{-1}. The IR spectrum related to the MW-HTC nanospheres (b panel, blue trace) exhibits glucose-like character (main band at 1000 cm^{-1} associated with C-O stretching of primary alcohols, although slightly lower in intensity compared to the black line). However, it also highlights new structures at 1650 cm^{-1}, indicative of water incorporation during the heat treatment and the development of new carbonyl (C=O) structures, as well as traces of aromatics (aromatic C-C at 1600-1500 cm^{-1}). Furthermore, the increased relative intensity of structures between 1400 and 1150 cm^{-1} suggests polymerization into various high molecular weight components through glucose caramelization, with these new structures coexisting with traces amounts of unreacted glucose [13].

The differences between the IR spectrum of MW-HTC particles and that of glucose monomers are accentuated in the case of the T-HTC nanospheres IR spectrum (panel c, red trace). In this case, the band at 1000 cm-1 has much lower relative intensity, and the spectrum is dominated by complex new structures, as evidenced by the high relative intensity of bands at 1700, 1615, 1280, and 1180 cm^{-1}. This is a clear fingerprint of the carbon network cross-linking [23], also involving aromatic species and presumably numerous lateral O-H side groups (note the difference between O-H stretching and bending signals in the spectrum of panel c) [24].

4. Conclusions

The FTIR characterization of the carbonaceous nanoparticles aligns with the structural and electrochemical analysis obtained from SEM and electrochemical experiments. The morphologies and surface chemistries resulting from the two different thermal treatments have been proved as a key factor influencing the efficacy of the Oxygen Reduction Reaction (ORR). The microwave-assisted hydrothermal carbonization (MW-HTC) method, despite its rapid processing capability, yields products with a surface chemistry and morphology that are less conducive to ORR when compared to those produced by the conventional hydrothermal carbonization (T-HTC) method. The T-HTC method facilitates a higher degree of carbonization, which appears to enhance the catalyst's effect on ORR. While the MW-HTC offers the advantage of speed of process, our study demonstrate the T-HTC as products with superior ORR performance due to a beneficial combination of surface chemistry and structural morphology. This research highlights the importance of considering how different synthesis methods affect the final product's ability to catalyze the ORR, explaining the need for fine-tuning the synthesis process to improve the performance of metal-free carbon catalysts.

Author Contributions: Conceptualization, C.F. and A.G.; methodology, A.S. and R.G.; formal analysis, C.M., A.S. and C.F.; resources, R.G. and M.I.; writing—original draft preparation, A.G., A.S. and C.M.; writing—review and editing, A.S. ad C.M.; supervision, C.F.; All authors have read and agreed to the published version of the manuscript.

Funding: C.F. gratefully thanks financial support from Ministry of University ad Research (MUR), PRIN 2022 cod. 2022NW4P2T "From metal nanoparticles to molecular complexes in electrocatalysis for green hydrogen evolution and simultaneous fine chemicals production (FUTURO)" and from Fondazione di Modena, Fondo di Ateneo per la Ricerca Anno 2023, linea FOMO, Progetto AMNESIA and from Consorzio Interuniversitario Nazionale per la Scienza e Tecnologia dei Materiali (INSTM), fondi triennali: "INSTM21MOFONTANESI".

Conflicts of Interest: The authors declare no conflict of interest.

References

1. T. J. Schmidt, V. Stamenkovic, J. P. N. Ross, and N. M. Markovic, 'Temperature dependent surface electrochemistry on Pt single crystals in alkaline electrolyte', *Phys. Chem. Chem. Phys.*, vol. 5, no. 2, pp. 400–406, Jan. 2003, doi: 10.1039/B208322A.
2. N. Ramaswamy and S. Mukerjee, 'Influence of Inner- and Outer-Sphere Electron Transfer Mechanisms during Electrocatalysis of Oxygen Reduction in Alkaline Media', *J. Phys. Chem. C*, vol. 115, no. 36, pp. 18015–18026, Sep. 2011, doi: 10.1021/jp204680p.
3. L. Zhang, H. Li, and J. Zhang, 'Kinetics of oxygen reduction reaction on three different Pt surfaces of Pt/C catalyst analyzed by rotating ring-disk electrode in acidic solution', *J. Power Sources*, vol. 255, pp. 242–250, Jun. 2014, doi: 10.1016/j.jpowsour.2014.01.042.
4. M. L. Pegis, C. F. Wise, D. J. Martin, and J. M. Mayer, 'Oxygen Reduction by Homogeneous Molecular Catalysts and Electrocatalysts', *Chem. Rev.*, vol. 118, no. 5, pp. 2340–2391, Mar. 2018, doi: 10.1021/acs.chemrev.7b00542.
5. Q. M. Yu-Wu, E. Weiss-Hortala, and R. Barna, 'Hydrothermal conversion of glucose in multiscale batch processes. Analysis of the gas, liquid and solid residues', *J. Supercrit. Fluids*, vol. 79, pp. 76–83, Jul. 2013, doi: 10.1016/j.supflu.2013.03.003.
6. E. Tovar-Martinez, C. E. Sanchez-Rodriguez, J. D. Sanchez-Vasquez, M. Reyes-Reyes, and R. López-Sandoval, 'Synthesis of carbon spheres from glucose using the hydrothermal carbonization method for the fabrication of EDLCs', *Diam. Relat. Mater.*, vol. 136, p. 110010, Jun. 2023, doi: 10.1016/j.diamond.2023.110010.
7. W. Zhang, J. Li, and Z. Wei, 'Carbon-based catalysts of the oxygen reduction reaction: Mechanistic understanding and porous structures', *Chin. J. Catal.*, vol. 48, pp. 15–31, May 2023, doi: 10.1016/S1872-2067(23)64427-4.
8. S. Guo *et al.*, 'Water-catalyzed conversion of glucose to small molecules during hydrothermal carbonization: a density functional theory study', *Sustain. Energy Fuels*, vol. 7, no. 5, pp. 1322–1332, Feb. 2023, doi: 10.1039/D2SE01733D.
9. M. Wang *et al.*, 'Iron oxide and phosphide encapsulated within N,P-doped microporous carbon nanofibers as advanced tri-functional electrocatalyst toward oxygen reduction/evolution and hydrogen evolution reactions and zinc-air batteries', *J. Power Sources*, vol. 413, pp. 367–375, Feb. 2019, doi: 10.1016/j.jpowsour.2018.12.056.
10. W. Yang, Y. Dong, J. Li, Q. Fu, and L. Zhang, 'Templating synthesis of hierarchically meso/macroporous N-doped microalgae derived biocarbon as oxygen reduction reaction catalyst for microbial fuel cells', *Int. J. Hydrog. Energy*, vol. 46, no. 2, pp. 2530–2542, Jan. 2021, doi: 10.1016/j.ijhydene.2020.10.087.
11. Q. He, J. Li, Y. Qiao, S. Zhan, and F. Zhou, 'Investigation of two-electron ORR pathway of non-metallic carbon-based catalysts with P-C bond structure in Cl--bearing electrolytes', *Appl. Catal. B Environ.*, vol. 339, p. 123087, Dec. 2023, doi: 10.1016/j.apcatb.2023.123087.
12. Y. Sang *et al.*, 'Chirality enhances oxygen reduction', *Proc. Natl. Acad. Sci.*, vol. 119, no. 30, p. e2202650119, Jul. 2022, doi: 10.1073/pnas.2202650119.
13. G. Ischia *et al.*, 'Hydrothermal carbonization of glucose: Secondary char properties, reaction pathways, and kinetics', *Chem. Eng. J.*, vol. 449, p. 137827, Dec. 2022, doi: 10.1016/j.cej.2022.137827.
14. S. E. Elaigwu and G. M. Greenway, 'Chemical, structural and energy properties of hydrochars from microwave-assisted hydrothermal carbonization of glucose', *Int. J. Ind. Chem.*, vol. 7, no. 4, pp. 449–456, Dec. 2016, doi: 10.1007/s40090-016-0081-0.
15. N. Abdulwali, J. Van Der Zalm, A. R. Thiruppathi, A. Khaleel, and A. Chen, 'Microwave-assisted green synthesis of monodispersed carbon micro-spheres and their antibacterial activity', *Appl. Surf. Sci.*, vol. 642, p. 158579, Jan. 2024, doi: 10.1016/j.apsusc.2023.158579.
16. E. S. Seven *et al.*, 'Hydrothermal vs microwave nanoarchitechtonics of carbon dots significantly affects the structure, physicochemical properties, and anti-cancer activity against a specific neuroblastoma cell line', *J. Colloid Interface Sci.*, vol. 630, pp. 306–321, Jan. 2023, doi: 10.1016/j.jcis.2022.10.010.
17. J. Poerschmann, B. Weiner, R. Koehler, and F.-D. Kopinke, 'Hydrothermal Carbonization of Glucose, Fructose, and Xylose—Identification of Organic Products with Medium Molecular Masses', *ACS Sustain. Chem. Eng.*, vol. 5, no. 8, pp. 6420–6428, Aug. 2017, doi: 10.1021/acssuschemeng.7b00276.
18. J. Peng *et al.*, 'Growth mechanism of glucose-based hydrochar under the effects of acid and temperature regulation', *J. Colloid Interface Sci.*, vol. 630, pp. 654–665, Jan. 2023, doi: 10.1016/j.jcis.2022.10.044.

19. B. C. Smith, 'An IR Spectral Interpretation Potpourri: Carbohydrates and Alkynes', *Spectroscopy*, vol. 32, no. 7, pp. 18–24, Jul. 2017, Accessed: Nov. 03, 2023. [Online]. Available: https://www.spectroscopyonline.com/view/ir-spectral-interpretation-potpourri-carbohydrates-and-alkynes
20. K. Bilba and A. Ouensanga, 'Fourier transform infrared spectroscopic study of thermal degradation of sugar cane bagasse', *J. Anal. Appl. Pyrolysis*, vol. 38, no. 1, pp. 61–73, Dec. 1996, doi: 10.1016/S0165-2370(96)00952-7.
21. M. Ibrahim, M. Alaam, H. El-Haes, A. F. Jalbout, and A. de Leon, 'Analysis of the structure and vibrational spectra of glucose and fructose', *Eclética Quím.*, vol. 31, pp. 15–21, 2006, doi: 10.1590/S0100-46702006000300002.
22. A. Nafar, 'Rapid green biosynthesis and characterization of silver nanoparticles using glucose as a green route', *Rev. Roum. Chim.*, Accessed: Nov. 03, 2023. [Online]. Available: https://www.academia.edu/65089637/Rapid_green_biosynthesis_and_characterization_of_silver_nanoparticles_using_glucose_as_a_green_route
23. Z. Fang, R. L. Smith, J. A. Kozinski, T. Minowa, and K. Arai, 'Reaction of d-glucose in water at high temperatures (410°C) and pressures (180MPa) for the production of dyes and nano-particles', *J. Supercrit. Fluids*, vol. 56, no. 1, pp. 41–47, Feb. 2011, doi: 10.1016/j.supflu.2010.11.009.
24. M. Li, W. Li, and S. Liu, 'Hydrothermal synthesis, characterization, and KOH activation of carbon spheres from glucose', *Carbohydr. Res.*, vol. 346, no. 8, pp. 999–1004, Jun. 2011, doi: 10.1016/j.carres.2011.03.020.